Struct Multidisc Optim (2013) 47:399–408
DOI 10.1007/s00158-012-0831-3

RESEARCH PAPER

Topology optimization to minimize the dynamic compliance of a bi-material plate in a thermal environment

Xiongwei Yang · Yueming Li

Received: 2 February 2012 / Revised: 9 June 2012 / Accepted: 16 July 2012 / Published online: 26 August 2012
© Springer-Verlag 2012

Abstract Topology optimization to minimize the structural dynamic compliance in a thermal environment is carried out in this paper. A bi-material plate subjected to a uniform temperature rise is investigated. The structure is driven by a time-harmonic surface loading with prescribed excitation frequency and amplitude. The stress induced by the equivalent thermal force which is known as design-dependent load could reduce the stiffness of the structure, thus altering the optimal topology design. A way to carry out the optimization in the thermal environments is presented here. The thermal stress is first evaluated, and then considered as pre-stress in the subsequent dynamic analysis with the introduction of the geometric stiffness matrix. The sensitivity analysis is carried out through adjoint method which can save significant computational resources by avoiding the derivatives of the thermal displacement (or thermal stress) on the design variables. The cost to obtain these derivatives can be very high since each design variable affects all the nodal displacements. The structural damping is neglected. Several pre-buckling cases are investigated.

Keywords Topology optimization · Dynamic compliance · Thermal environment

National Natural Science Foundation of China (91016008,11021202)

X. Yang · Y. Li (✉)
State Key Laboratory for Strength and Vibration of Mechanical Structures, School of Aerospace, Xi'an Jiaotong University, Xi'an Shaanxi 710049, People's Republic of China
e-mail: liyueming@mail.xjtu.edu.cn

1 Introduction

One of the problems encountered by the hypersonic vehicles is the high thermal environment to which the aircraft is subjected during a significant portion of the flight envelope. Severe thermal environment due to the aerodynamic heating induces compressive stresses which could alter the dynamic characteristic and even cause thermal buckling. Thus, the structural design for the spacecraft operating in such extreme environment is of significant importance to provide light-weight structures with good dynamic properties under thermal conditions.

Topology optimization has been extended to dynamic field to find the optimal configurations of structures with respect to different dynamic criteria since the landmark work of Bendsøe and Kikuchi (1988). Diaz and Kikuchi (1992) first studied the shape and topology optimization of structures to maximize a natural frequency using homogenization method. Ma et al. (1993, 1995), Min et al. (1999) applied the homogenization method to vibrating structures. ESO (Evolutionary Structural Optimization) was employed to optimization problems with frequency constraints (Xie and Steven 1996) and dynamic loads (Huang et al. 2010). Jog (2002) studied the topology configuration of structures subjected to periodic loadings from the global and local dynamic constraints. Du and Olhoff (2007b) employed SIMP (Solid Isotropic Material with Penalization) to maximize the eigenfrequency of higher order, or the gap between two consecutive eigenfrequencies of given orders.

One of other challenging research fields is the topological design involving so-called design-dependent loads (Rozvany 2001; Bruyneel and Duysinx 2005; Gao and Zhang 2010), of which the thermal load is a typical one (Gao and Zhang 2010). Rodrigues and Fernandes (1995) first studied the topology optimization of a 2-D linear-elastic

solid subjected to thermal loads. Li et al. (1999) employed ESO to minimize the displacement under thermal and mechanical loading. Kim et al. (2006) and Penmetsa et al. (2006) applied ESO in the topological design of thermal protection system of spacecraft. A particular characteristic of the thermal load is that it concerns both the elastic modulus and the thermal expansion coefficient. For a bi-material structural topology optimization, the penalties of these two parameters should match each other; otherwise incompatibility may occur for intermediate densities between stiffness and thermal load during the optimization. Gao and Zhang (2010) characterized the design-dependent property of thermal-load by penalizing the thermal stress coefficient, i.e. the product of elastic modulus and thermal expansion coefficient, which in fact can be found in Rodrigues and Fernandes (1995).

It is well known that thermal stress may change the stiffness of structure, thus altering the dynamic characteristic (Zienkiewicz and Taylor 2005). Things become more interesting when the effect of thermal stress is taken into account in the dynamic optimization.

Literature survey shows that limited work has been done to study the effect of the thermal environments on the structural dynamic topology optimization. A common way to study the dynamic characteristic of structures subjected to some particular environment is to treat the initial stress as pre-tress. Pedersen (2001, 2002) optimized the static compliance or eigenvalues of pre-stressed isotropic and laminated plates in MEMS design. The stresses were given at different values to study its influence on the topology. In fact, these thermal stresses are constantly changing during the optimization.

In this paper, topology optimization with respect to the dynamic compliance of a bi-material plate subjected to a uniform thermal environment and driven by a time-harmonic surface load is carried out. The dynamic surface load is of prescribed excitation frequency and amplitude. The critical buckling temperature is first evaluated to determine the upper limit of the temperature rise, so that a pre-buckling small-deformation could be assumed to establish the dynamic formula in a stress stiffening form (Cook 1994). The thermal stress is then calculated and used to form the geometric stiffness matrix to obtain the thermal dynamic equation. Both direct and adjoint methods are discussed, and the adjoint method is implemented to carry out the sensitivity analysis, which is much more computational-economical than the direct method; accordingly the optimization is carried out. During the optimization, the critical buckling temperature is monitored to check whether the structure is in the pre-buckling state.

The thermal stress coefficient (Rodrigues and Fernandes 1995; Gao and Zhang 2010) is employed to characterize the equivalent thermal force. The RAMP (Rational Approximation of Material Properties) interpolation model (Stolpe and Svanberg 2001) and GCMMA (Svanberg 1995), the globally convergent version of MMA (Method of Moving Asymptotes) (Svanberg 1987) are used in this paper.

The paper is organized as follows. Finite element formulas for dynamic structure in a thermal environment are presented in the next section. Then the optimization problem is detailed in Section 3, followed by the sensitivity analysis in Section 4. Finally some optimization cases are presented and discussed in Section 5.

2 Dynamic structure in a thermal environment

2.1 Buckling analysis

When a plate is subjected to temperature rise from the ambient, thermal stress develops. The thermal stress may induce buckling of the structure when the temperature change is high enough. The optimization is carried out when the plate is in the pre-buckling state; thus, the critical buckling temperature T_{cr} is first evaluated to determine the upper limit of the uniform temperature rise. An eigenvalue buckling analysis could be stated as (Cook 1994)

$$(\mathbf{K} + \lambda \mathbf{K}_{\mathrm{G}})\, \boldsymbol{\Phi} = \mathbf{0} \tag{1}$$

where λ is a scalar multiplier, $\boldsymbol{\Phi}$ is the eigenvector and $\mathbf{K}$ is the stiffness matrix. $\Delta T = T_1 - T_0$ is the temperature change.

$$T_{\mathrm{cr}} = T_0 + \lambda \Delta T \tag{2}$$

$\mathbf{K}_{\mathrm{G}}$ refers to the geometric stiffness for bending induced by the in-plane thermal stress (Zienkiewicz and Taylor 2005)

$$\mathbf{K}_{\mathrm{G}} = \sum_i \int_{A_i} \mathbf{G}^{\mathrm{T}} \mathbf{S} \mathbf{G}\, dA \tag{3}$$

where $\mathbf{S}$ is the membrane stress matrix at the element level; $\mathbf{G}$ is a strain-displacement matrix; A_i is the area of the element.

2.2 Membrane stress analysis

If the temperature change across the thickness is uniform, the thermo-elastic problem of the plate could be described by the plane-stress constitutive equation,

$$\boldsymbol{\sigma} = \mathbf{D}_{\mathrm{m}} (\boldsymbol{\varepsilon} - \alpha \Delta \mathbf{T}) = E \mathbf{D} \boldsymbol{\varepsilon} - \beta \mathbf{D} \Delta \mathbf{T} \tag{4}$$

where $\boldsymbol{\sigma}$ is the membrane stress vector; $E, \alpha, \beta{=}E\alpha$ are the elastic modulus, the thermal expansion coefficient and the thermal stress coefficient respectively; $\mathbf{D}_\mathrm{m}$ is the membrane elasticity matrix; $\Delta\mathbf{T}$ is the temperature rise vector.

The strain in (4) could be written in FE form

$$\boldsymbol{\varepsilon} = \mathbf{B}\mathbf{U}_{ti} \tag{5}$$

where $\mathbf{B}$ is the strain-displacement matrix; $\mathbf{U}_{ti}$ is the displacement vector of element i, which could be obtained with the boundary conditions through

$$\mathbf{K}\mathbf{U}_\mathrm{t} = \mathbf{F}_\mathrm{t} \tag{6}$$

where $\mathbf{F}_\mathrm{t}$ is the equivalent thermal force induced by the uniform temperature rise; $\mathbf{U}_\mathrm{t}$ is the thermal displacement; the index "t" denotes the word "thermal".

The equivalent membrane thermal force $\mathbf{F}_\mathrm{t}$ has the form (Zienkiewicz and Taylor 2005)

$$\begin{aligned}\mathbf{F}_\mathrm{t} &= -\sum_i \int_{A_i} \alpha \mathbf{B}^\mathrm{T}\mathbf{D}_\mathrm{m}\Delta\mathbf{T}\,dA \\ &= -\sum_i \int_{A_i} \beta \mathbf{B}^\mathrm{T}\mathbf{D}\Delta\mathbf{T}\,dA\end{aligned} \tag{7}$$

Equation (7) indicates that the equivalent thermal force is design-dependent, related to the thermal stress coefficient β. The relationship between $\mathbf{F}_\mathrm{t}$ and the interpolation function (that is, $R(\zeta)$ in (12)) will be quadratic if the thermal stress coefficient $\beta{=}E\alpha$ is not introduced. Since K is the linear function of $R(\zeta)$, incompatibility may occur between the stiffness and the thermal load. By employing the thermal stress coefficient β, the penalty could be made properly to the thermal load $\mathbf{F}_\mathrm{t}$, and the incompatibility could be efficiently avoided (Rodrigues and Fernandes 1995; Gao and Zhang 2010).

2.3 Dynamic formula

When the thermal load is below T_cr, the dynamic finite element formula of the plate in a uniform thermal environment could be written in a stress stiffening form (the damping is neglected) (Cook 1994)

$$\left(\mathbf{K} + \mathbf{K}_\mathrm{G} - \omega^2\mathbf{M}\right)\mathbf{U} = \mathbf{F} \tag{8}$$

where $\mathbf{K}, \mathbf{M}$ are the stiffness and mass matrices respectively; $\mathbf{F}$ is the amplitude vector of the time-harmonic external load; $\omega = 2\pi f$ is the angular frequency; $\mathbf{U}$ is the dynamic displacement response vector.

3 Optimization problem

3.1 Problem formulation

Ma et al. (1995) defined the dynamic compliance of an undamped structure as the product of the time-harmonic force and the displacement vectors, that is

$$C = \mathbf{F}^\mathrm{T}\mathbf{U} \tag{9}$$

As pointed out by Jog (2002), the dynamic compliance becomes negative if the excitation frequency is slightly higher than the fundamental frequency; minimization of this function drives the system towards resonance instead of away from it.

A way to avoid this is to minimize the square of the product (Bendsøe and Sigmund 2003), that is

$$C = \left\{\mathbf{F}^\mathrm{T}\mathbf{U}\right\}^2 \tag{10}$$

Thus the dynamic topology optimization problem in the thermal environment could be stated as

$$\begin{aligned}\min\ & C = \left\{\mathbf{F}^\mathrm{T}\mathbf{U}\right\}^2 \\ s.t.\ & \left(\mathbf{K} + \mathbf{K}_\mathrm{G} - \omega^2\mathbf{M}\right)\mathbf{U} = \mathbf{F} \\ & \mathbf{K}\mathbf{U}_\mathrm{t} = \mathbf{F}_\mathrm{t} \\ & \sum_i^n V_i\zeta_i \le V^{(1)} \\ & \zeta_i \in (0, 1)\end{aligned} \tag{11}$$

where ζ_i is the design variable, denoting the artificial volume fraction of material 1 (the stiffer one of the two materials) in the element i; n is the total number of the elements; V_i is the volume of the element i; $V^{(1)}$ is the maximum volume of material 1 in the structure. At each iteration, the second constraint equation is first assembled and solved to calculate the thermal displacement $\mathbf{U}_\mathrm{t}$. With (4) and (5), the membrane thermal stress $\boldsymbol{\sigma}$ can be obtained to get the geometric stiffness matrix $\mathbf{K}_\mathrm{G}$. The first constraint equation can then be solved.

3.2 Interpolation model

It has been shown (Pedersen 2000; Bruyneel and Duysinx 2005; Gao and Zhang 2010) that the volume constraint may not be a binding one in SIMP interpolation model and the compliance becomes unbounded in low-density regions for design-dependent problems. The reason is that SIMP has a zero-slope at $\zeta = 0$.

RAMP proposed by Stolpe and Svanberg (2001) turns out to be effective in dealing with such difficulty (Bruyneel

and Duysinx 2005; Gao and Zhang 2010) (A more flexible interpolation model NLPI, can be found in Pedersen and Pedersen (2012)). The RAMP interpolation models of the elastic modulus, the mass density and the thermal stress coefficient can be written as

$$E_i = R(\zeta_i) E^{(1)} + (1 - R(\zeta_i)) E^{(0)} \tag{12}$$

$$\rho_i = R(\zeta_i) \rho^{(1)} + (1 - R(\zeta_i)) \rho^{(0)} \tag{13}$$

$$\beta_i = R(\zeta_i) \beta^{(1)} + (1 - R(\zeta_i)) \beta^{(0)} \tag{14}$$

where the superscripts 0 and 1 denote material 0 and material 1 respectively;

$$R(\zeta_i) = \frac{\zeta_i}{1 + p(1 - \zeta_i)} \tag{15}$$

and p is the penalty factor.

4 Sensitivity analysis

The sensitivity could be written as

$$\frac{\mathrm{d}C}{\mathrm{d}\zeta_i} = \boldsymbol{\Psi}^{\mathrm{T}} \left(\frac{\mathrm{d}\mathbf{K}}{\mathrm{d}\zeta_i} + \frac{\mathrm{d}\mathbf{K}_{\mathrm{G}}}{\mathrm{d}\zeta_i} - \omega^2 \frac{\mathrm{d}\mathbf{M}}{\mathrm{d}\zeta_i} \right) \mathbf{U} \tag{16}$$

where $\boldsymbol{\Psi}$ is the solution of the problem

$$\left(\mathbf{K} + \mathbf{K}_{\mathrm{G}} - \omega^2 \mathbf{M} \right) \boldsymbol{\Psi} = -2 \left\{ \mathbf{F}^{\mathrm{T}} \mathbf{U} \right\} \mathbf{F} \tag{17}$$

Note that $\mathbf{K}_{\mathrm{G}}$ is symmetric since the membrane stress $\mathbf{S}$ is symmetric (Zienkiewicz and Taylor 2005).

The key to the sensitivity analysis is how to deal with the derivative of the geometric stiffness matrix $\mathbf{K}_{\mathrm{G}}$, since it involves not only the temperature change, but also the strain induced by the design-dependent equivalent thermal force, see (3) and (4). Furthermore, the strain of element j is related to all the design variables and so is the $\mathbf{K}_{\mathrm{G}j}$.

Equation (16) can be written as

$$\frac{\mathrm{d}C}{\mathrm{d}\zeta_i} = \boldsymbol{\Psi}_i^{\mathrm{T}} \left(\frac{\mathrm{d}\mathbf{K}_i}{\mathrm{d}\zeta_i} - \omega^2 \frac{\mathrm{d}\mathbf{M}_i}{\mathrm{d}\zeta_i} \right) \mathbf{U}_i + \sum_j^n \boldsymbol{\Psi}_j^{\mathrm{T}} \frac{\mathrm{d}\mathbf{K}_{\mathrm{G}j}}{\mathrm{d}\zeta_i} \mathbf{U}_j \tag{18}$$

In this paper, both direct method and adjoint method are discussed.

4.1 Derivatives of stiffness and mass matrices

The derivatives of $\mathbf{K}_i$ and $\mathbf{M}_i$ in (18) are as follows,

$$\frac{\mathrm{d}\mathbf{K}_i}{\mathrm{d}\zeta_i} = \frac{1 + p}{(1 + p(1 - \zeta_i))^2} \left(\mathbf{K}_i^{(1)} - \mathbf{K}_i^{(0)} \right) \tag{19}$$

$$\frac{\mathrm{d}\mathbf{M}_i}{\mathrm{d}\zeta_i} = \frac{1 + p}{(1 + p(1 - \zeta_i))^2} \left(\mathbf{M}_i^{(1)} - \mathbf{M}_i^{(0)} \right) \tag{20}$$

4.2 Direct method

According to (4), the membrane stress in (3) could be stated as

$$S = E\boldsymbol{\Xi} - \beta\boldsymbol{\Theta} \tag{21}$$

where $E\boldsymbol{\Xi}$ and $\beta\boldsymbol{\Theta}$ refer to the strain part and the thermal expansion part respectively. Since $\mathrm{K}_{\mathrm{G}j}$ is only related to the membrane stress of the element j, it could be divided as follows,

$$\begin{aligned} \mathbf{K}_{\mathrm{G}j} &= \int_{A_j} \mathbf{G}^{\mathrm{T}} \mathbf{S} \mathbf{G} dA \\ &= \int_{A_j} \mathbf{G}^{\mathrm{T}} \left(E_j \boldsymbol{\Xi} - \beta_j \boldsymbol{\Theta} \right) \mathbf{G} dA \\ &= \int_{A_j} E_j \mathbf{G}^{\mathrm{T}} \boldsymbol{\Xi} \mathbf{G} dA - \int_{A_j} \beta_j \mathbf{G}^{\mathrm{T}} \boldsymbol{\Theta} \mathbf{G} dA \\ &= \mathbf{K}_{\mathrm{G}j}^{\mathrm{I}} + \mathbf{K}_{\mathrm{G}j}^{\mathrm{II}} \end{aligned} \tag{22}$$

Accordingly the derivative of $\mathrm{K}_{\mathrm{G}j}$ could be written as

$$\begin{aligned} \frac{\mathrm{d}\mathbf{K}_{\mathrm{G}j}}{\mathrm{d}\zeta_i} &= \frac{\mathrm{d}\mathbf{K}_{\mathrm{G}j}^{\mathrm{I}}}{\mathrm{d}\zeta_i} + \frac{\mathrm{d}\mathbf{K}_{\mathrm{G}j}^{\mathrm{II}}}{\mathrm{d}\zeta_i} \\ &= \frac{\mathrm{d}E_j}{\mathrm{d}\zeta_i} \int_{A_j} \mathbf{G}^{\mathrm{T}} \boldsymbol{\Xi} \mathbf{G} dA \\ &\quad + E_j \int_{A_j} \mathbf{G}^{\mathrm{T}} \frac{\mathrm{d}\boldsymbol{\Xi}}{\mathrm{d}\zeta_i} \mathbf{G} dA \\ &\quad - \frac{\mathrm{d}\beta_j}{\mathrm{d}\zeta_i} \int_{A_j} \mathbf{G}^{\mathrm{T}} \boldsymbol{\Theta} \mathbf{G} dA \end{aligned} \tag{23}$$

$\mathrm{d}E_j/\mathrm{d}\zeta_i$, $\mathrm{d}\beta_j/\mathrm{d}\zeta_i$ can be obtained with (12) and (14) when $i = j$, and equal 0 when $i \neq j$.It can be found that only the second part of the right-hand items is left to deal with. Since the membrane stress S has been stated as (21) according to (4); the derivative of $\boldsymbol{\Xi}$ is in fact equivalent to the derivative of $\boldsymbol{\varepsilon}$; both refer to the derivatives of the membrane strains. With (5), the derivative is shown as,

$$\frac{\mathrm{d}\boldsymbol{\varepsilon}_j}{\mathrm{d}\zeta_i} = \frac{\mathrm{d}\left(\mathbf{B}\mathbf{U}_{\mathrm{t}j}\right)}{\mathrm{d}\zeta_i} = \mathbf{B} \frac{\mathrm{d}\mathbf{U}_{\mathrm{t}j}}{\mathrm{d}\zeta_i} \tag{24}$$

Differentiate (6) as follows

$$\frac{\mathrm{d}\left(\mathbf{K}\mathbf{U}_{\mathrm{t}}\right)}{\mathrm{d}\zeta_i} = \frac{\mathrm{d}\mathbf{F}_{\mathrm{t}}}{\mathrm{d}\zeta_i} \tag{25}$$

$$\mathbf{K}_j \frac{\mathrm{d}\mathbf{U}_{\mathrm{t}j}}{\mathrm{d}\zeta_i} = -\frac{\mathrm{d}\mathbf{K}_j}{\mathrm{d}\zeta_i} \mathbf{U}_{\mathrm{t}j} + \frac{\mathrm{d}\mathbf{F}_{\mathrm{t}j}}{\mathrm{d}\zeta_i} \tag{26}$$

Note that $\mathrm{d}\mathbf{F}_{\mathrm{t}j}/\mathrm{d}\zeta_i$ equal $\mathbf{0}$ when $i \neq j$,

$$\frac{\mathrm{d}\mathbf{F}_{\mathrm{t}i}}{\mathrm{d}\zeta_i} = \frac{\mathrm{d}\beta_i}{\mathrm{d}\zeta_i} \int_{A_i} \mathbf{B}^{\mathrm{T}} \mathbf{D} \Delta \mathbf{T} dA \tag{27}$$

In this direct method, the computer cost can be huge for large-scale problems, since (26) needs to be solved for the sensitivity on each design variable in every iteration.

4.3 Adjoint method

It can be seen from (23) $\mathbf{K}_\mathrm{G}$ is the function of $\mathbf{U}_\mathrm{t}$, E, β, ζ, so (16) can be rewritten as

$$\frac{\mathrm{d}C}{\mathrm{d}\zeta_i} = \boldsymbol{\Psi}^\mathrm{T}\left(\frac{\mathrm{d}\mathbf{K}}{\mathrm{d}\zeta_i} - \omega^2\frac{\mathrm{d}\mathbf{M}}{\mathrm{d}\zeta_i}\right)\mathbf{U} + \boldsymbol{\Psi}^\mathrm{T}\left(\left(\frac{\partial\mathbf{K}_\mathrm{G}}{\partial\mathbf{U}_\mathrm{t}}\right)^\mathrm{T}\frac{\partial\mathbf{U}_\mathrm{t}}{\partial\zeta_i} + \frac{\partial\mathbf{K}_\mathrm{G}}{\partial\mathbf{E}}\frac{\partial\mathbf{E}}{\partial\zeta_i} + \frac{\partial\mathbf{K}_\mathrm{G}}{\partial\boldsymbol{\beta}}\frac{\partial\boldsymbol{\beta}}{\partial\zeta_i}\right)\mathbf{U} \tag{28}$$

where $\mathbf{E}$=(E_1, E_2,…,E_n), $\boldsymbol{\beta}$=(β_1,β_2,…,β_n) are the vectors of the elastic modulus and the thermal expansion coefficient respectively.

With the introduction of an adjoint vector $\boldsymbol{\Lambda}$ of the thermal displacement, (28) can be written as

$$\frac{\mathrm{d}C}{\mathrm{d}\zeta_i} = \boldsymbol{\Psi}^\mathrm{T}\left(\frac{\mathrm{d}\mathbf{K}}{\mathrm{d}\zeta_i} - \omega^2\frac{\mathrm{d}\mathbf{M}}{\mathrm{d}\zeta_i}\right)\mathbf{U} + \boldsymbol{\Psi}^\mathrm{T}\left(\left(\frac{\partial\mathbf{K}_\mathrm{G}}{\partial\mathbf{U}_\mathrm{t}}\right)^\mathrm{T}\frac{\partial\mathbf{U}_\mathrm{t}}{\partial\zeta_i} + \frac{\partial\mathbf{K}_\mathrm{G}}{\partial\mathbf{E}}\frac{\partial\mathbf{E}}{\partial\zeta_i} + \frac{\partial\mathbf{K}_\mathrm{G}}{\partial\boldsymbol{\beta}}\frac{\partial\boldsymbol{\beta}}{\partial\zeta_i}\right)\mathbf{U} + \boldsymbol{\Lambda}^\mathrm{T}\left(\mathbf{K}\frac{\mathrm{d}\mathbf{U}_\mathrm{t}}{\mathrm{d}\zeta_i} + \frac{\mathrm{d}\mathbf{K}}{\mathrm{d}\zeta_i}\mathbf{U}_\mathrm{t} - \frac{\mathrm{d}\mathbf{F}_\mathrm{t}}{\mathrm{d}\zeta_i}\right) \tag{29}$$

which can be rearranged as

$$\frac{\mathrm{d}C}{\mathrm{d}\zeta_i} = \boldsymbol{\Psi}^\mathrm{T}\left(\frac{\mathrm{d}\mathbf{K}}{\mathrm{d}\zeta_i} - \omega^2\frac{\mathrm{d}\mathbf{M}}{\mathrm{d}\zeta_i}\right)\mathbf{U} + \boldsymbol{\Psi}^\mathrm{T}\left(\frac{\partial\mathbf{K}_\mathrm{G}}{\partial\mathbf{E}}\frac{\partial\mathbf{E}}{\partial\zeta_i} + \frac{\partial\mathbf{K}_\mathrm{G}}{\partial\boldsymbol{\beta}}\frac{\partial\boldsymbol{\beta}}{\partial\zeta_i}\right)\mathbf{U} + \boldsymbol{\Lambda}^\mathrm{T}\left(\frac{\mathrm{d}\mathbf{K}}{\mathrm{d}\zeta_i}\mathbf{U}_\mathrm{t} - \frac{\mathrm{d}\mathbf{F}_\mathrm{t}}{\mathrm{d}\zeta_i}\right) + \boldsymbol{\Lambda}^\mathrm{T}\mathbf{K}\frac{\mathrm{d}\mathbf{U}_\mathrm{t}}{\mathrm{d}\zeta_i} + \boldsymbol{\Psi}^\mathrm{T}\left(\frac{\partial\mathbf{K}_\mathrm{G}}{\partial\mathbf{U}_\mathrm{t}}\right)^\mathrm{T}\frac{\partial\mathbf{U}_\mathrm{t}}{\partial\zeta_i}\mathbf{U} \tag{30}$$

In order to avoid the computation of $\partial\mathbf{U}_\mathrm{t}/\partial\zeta_i$,

$$\boldsymbol{\Lambda}^\mathrm{T}\mathbf{K}\frac{\mathrm{d}\mathbf{U}_\mathrm{t}}{\mathrm{d}\zeta_i} + \boldsymbol{\Psi}^\mathrm{T}\left(\frac{\partial\mathbf{K}_\mathrm{G}}{\partial\mathbf{U}_\mathrm{t}}\right)^\mathrm{T}\frac{\partial\mathbf{U}_\mathrm{t}}{\partial\zeta_i}\mathbf{U} = \mathbf{0} \tag{31}$$

Thus, (30) can be simplified to

$$\frac{\mathrm{d}C}{\mathrm{d}\zeta_i} = \boldsymbol{\Psi}^\mathrm{T}\left(\frac{\mathrm{d}\mathbf{K}}{\mathrm{d}\zeta_i} - \omega^2\frac{\mathrm{d}\mathbf{M}}{\mathrm{d}\zeta_i}\right)\mathbf{U} + \boldsymbol{\Psi}^\mathrm{T}\left(\frac{\partial\mathbf{K}_\mathrm{G}}{\partial\mathbf{E}}\frac{\partial\mathbf{E}}{\partial\zeta_i} + \frac{\partial\mathbf{K}_\mathrm{G}}{\partial\boldsymbol{\beta}}\frac{\partial\boldsymbol{\beta}}{\partial\zeta_i}\right)\mathbf{U} + \boldsymbol{\Lambda}^\mathrm{T}\left(\frac{\mathrm{d}\mathbf{K}}{\mathrm{d}\zeta_i}\mathbf{U}_\mathrm{t} - \frac{\mathrm{d}\mathbf{F}_\mathrm{t}}{\mathrm{d}\zeta_i}\right) \tag{32}$$

This equation can be written at element level and please note that $\partial E_j/\partial\zeta_i$, $\partial\beta_j/\partial\zeta_i$, $\partial\mathbf{K}_j/\partial\zeta_i$, $\partial\mathbf{M}_j/\partial\zeta_i$,$\partial\mathbf{F}_{\mathrm{t}j}/\partial\zeta_i$ equal 0 when $i \neq j$

$$\frac{\mathrm{d}C}{\mathrm{d}\zeta_i} = \boldsymbol{\Psi}_i^\mathrm{T}\left(\frac{\mathrm{d}\mathbf{K}_i}{\mathrm{d}\zeta_i} + \frac{\partial\mathbf{K}_{\mathrm{G}i}}{\partial E_i}\frac{\partial E_i}{\partial\zeta_i} + \frac{\partial\mathbf{K}_{\mathrm{G}i}}{\partial\beta_i}\frac{\partial\beta_i}{\partial\zeta_i} - \omega^2\frac{\mathrm{d}\mathbf{M}_i}{\mathrm{d}\zeta_i}\right)\mathbf{U}_i + \boldsymbol{\Lambda}_i^\mathrm{T}\left(\frac{\mathrm{d}\mathbf{K}_i}{\mathrm{d}\zeta_i}\mathbf{U}_{\mathrm{t}i} - \frac{\mathrm{d}\mathbf{F}_{\mathrm{t}i}}{\mathrm{d}\zeta_i}\right) \tag{33}$$

Equation (31) can also be written at element level and please note that $\mathbf{U}_{\mathrm{t}j}$ only affects $\mathbf{K}_{\mathrm{G}j}$.

$$\boldsymbol{\Lambda}_j^\mathrm{T}\mathbf{K}_j\frac{\partial\mathbf{U}_{\mathrm{t}j}}{\partial\zeta_i} + \boldsymbol{\Psi}_j^\mathrm{T}\left(\frac{\partial\mathbf{K}_{\mathrm{G}j}}{\partial\mathbf{U}_{\mathrm{t}j}}\right)^\mathrm{T}\frac{\partial\mathbf{U}_{\mathrm{t}j}}{\partial\zeta_i}\mathbf{U}_j = 0 \tag{34}$$

in which

$$\left(\frac{\partial\mathbf{K}_{\mathrm{G}j}}{\partial\mathbf{U}_{\mathrm{t}j}}\right)^\mathrm{T}\frac{\partial\mathbf{U}_{\mathrm{t}j}}{\partial\zeta_i} = \frac{\partial\mathbf{K}_{\mathrm{G}j}}{\partial U_{\mathrm{t}j1}}\frac{\partial U_{\mathrm{t}j1}}{\partial\zeta_i} + \cdots + \frac{\partial\mathbf{K}_{\mathrm{G}j}}{\partial U_{\mathrm{t}jk}}\frac{\partial U_{\mathrm{t}jk}}{\partial\zeta_i} + \cdots + \frac{\partial\mathbf{K}_{\mathrm{G}j}}{\partial U_{\mathrm{t}jm}}\frac{\partial U_{\mathrm{t}jm}}{\partial\zeta_i} \tag{35}$$

where $U_{\mathrm{t}jk}$ refers to the thermal displacement at the kth DOF (degree of freedom) of jth element; m is the total DOF number of the jth element. Thus (34) can be written as

$$\boldsymbol{\Lambda}_j^\mathrm{T}\mathbf{K}_j\begin{Bmatrix}\frac{\partial U_{\mathrm{t}j1}}{\partial\zeta_i}\\ \frac{\partial U_{\mathrm{t}j2}}{\partial\zeta_i}\\ \vdots\\ \frac{\partial U_{\mathrm{t}jm}}{\partial\zeta_i}\end{Bmatrix} + \begin{Bmatrix}\boldsymbol{\Psi}_j^\mathrm{T}\left(\frac{\partial\mathbf{K}_{\mathrm{G}j}}{\partial U_{\mathrm{t}1}}\right)^\mathrm{T}\mathbf{U}_j\\ \boldsymbol{\Psi}_j^\mathrm{T}\left(\frac{\partial\mathbf{K}_{\mathrm{G}j}}{\partial U_{\mathrm{t}2}}\right)^\mathrm{T}\mathbf{U}_j\\ \vdots\\ \boldsymbol{\Psi}_j^\mathrm{T}\left(\frac{\partial\mathbf{K}_{\mathrm{G}j}}{\partial U_{\mathrm{t}m}}\right)^\mathrm{T}\mathbf{U}_j\end{Bmatrix}^\mathrm{T}\cdot\begin{Bmatrix}\frac{\partial U_{\mathrm{t}j1}}{\partial\zeta_i}\\ \frac{\partial U_{\mathrm{t}j2}}{\partial\zeta_i}\\ \vdots\\ \frac{\partial U_{\mathrm{t}jm}}{\partial\zeta_i}\end{Bmatrix} = 0 \tag{36}$$

that is,

$$\left(\mathbf{K}_j\boldsymbol{\Lambda}_j + \boldsymbol{\Psi}_j^\mathrm{T}\left(\frac{\partial\mathbf{K}_{\mathrm{G}j}}{\partial\mathbf{U}_{\mathrm{t}j}}\right)^\mathrm{T}\mathbf{U}_j\right)^\mathrm{T}\frac{\partial\mathbf{U}_{\mathrm{t}j}}{\partial\zeta_i} = 0 \tag{37}$$

Thus, $\boldsymbol{\Lambda}$ can be obtained by solving

$$\mathbf{K}\boldsymbol{\Lambda} = -\boldsymbol{\Psi}^\mathrm{T}\left\{\frac{\partial\mathbf{K}_\mathrm{G}}{\partial\mathbf{U}_\mathrm{t}}\right\}^\mathrm{T}\mathbf{U} \tag{38}$$

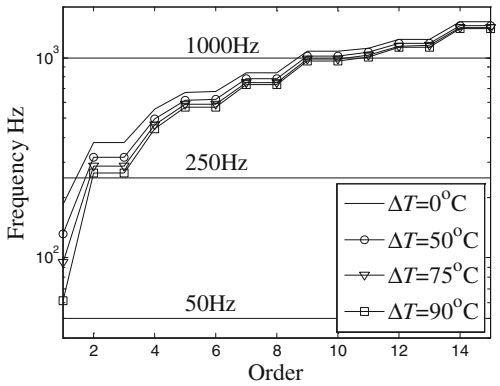

Fig. 1 First 15 natural frequencies and 3 excitation frequencies

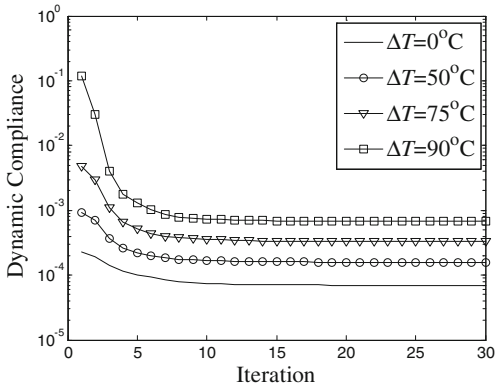

Fig. 3 Iteration history of the dynamic compliance of the case $f = 50$ Hz

As the relationship between $\mathbf{K}_{\mathrm{G}j}$ and $\mathbf{U}_{\mathrm{t}j}$ is linear (Zienkiewicz and Taylor 2005), $\partial \mathbf{K}_{\mathrm{G}j}/\partial \mathbf{U}_{\mathrm{t}j}$ can be obtained through

$$\frac{\partial \mathbf{K}_{\mathrm{G}j}}{\partial \mathbf{U}_{\mathrm{t}j}} = \frac{\mathbf{K}_{\mathrm{G}j}\left(\mathbf{U}_{\mathrm{t}j} + \Delta \mathbf{u}_j\right)}{\Delta \mathbf{u}_j} \tag{39}$$

where $\Delta \mathbf{u}_j$ is the displacement change at element j. The kth DOF component of (39) is

$$\frac{\partial \mathbf{K}_{\mathrm{G}j}}{\partial U_{\mathrm{t}jk}} = \frac{\mathbf{K}_{\mathrm{G}j}\left(U_{\mathrm{t}jk} + \Delta u_{jk}\right)}{\Delta u_{jk}} \tag{40}$$

By adjoint method, (38) needs to be solved only once in each iteration, and the computational cost can be effectively controlled.

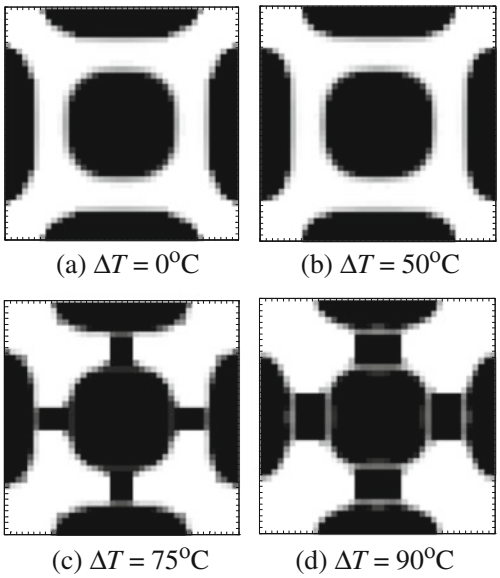

Fig. 2 Topology of the case $f = 50$ Hz (*white*: material 0; *black*: material 1)

5 Numerical examples

A four-edge clamped bi-material square plate with dimension 1 m × 1 m × 0.01 m is studied. The plate is subjected to a uniform temperature rise $\Delta T = T_1 - T_0$ with $T_0 = 0$ °C. The material properties are as follows:

$$E^{(0)} = 70\mathrm{GPa},\ \rho^{(0)} = 2650\mathrm{kg/m^3},\ \alpha^{(0)} = 1.5 \times 10^{-5}{}^{\circ}\mathrm{C}^{-1}$$

$$E^{(1)} = 210\mathrm{GPa},\ \rho^{(1)} = 6500\,\mathrm{kg/m^3},\ \alpha^{(1)} = 1.1 \times 10^{-5}{}^{\circ}\mathrm{C}^{-1}$$

A mesh of 40 × 40 with isoparametric 4-node element is used here, and there are 1600 design variables. The normal external surface loading is defined in such a way that unit concentrated force is applied to each node of the mesh.

The volume fraction of material 1 is up to 50 %, that is $V^{(1)}/V = 0.5$, where V is the volume of the plate. And the initial value of all the design variables is $\zeta_i = 0.5$.

Since (38) needs to be solved during the sensitivity analysis, the dynamic compliance may possibly be non-monotonous. GCMMA algorithm (Svanberg 1995) is employed.

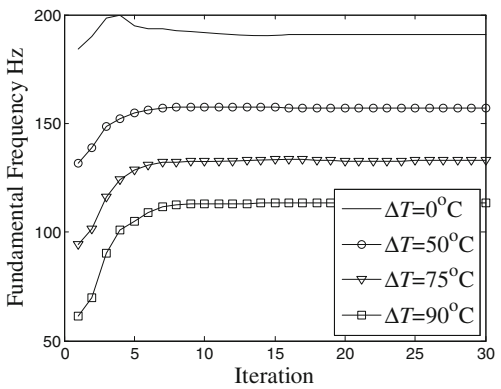

Fig. 4 Iteration history of the fundamental frequency of the case $f = 50$ Hz

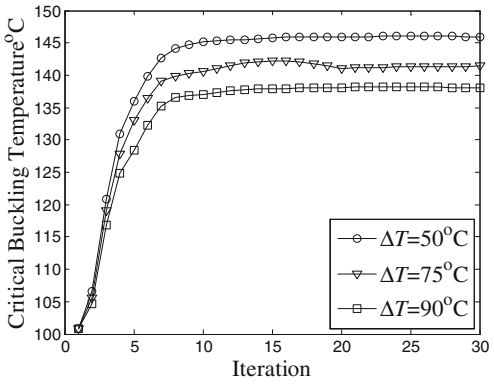

Fig. 5 Iteration history of the critical buckling temperature of the case $f = 50$ Hz

Filtering of the sensitivity is implemented to control the checkerboards (Sigmund 2001; Bendsøe and Sigmund 2003). The filtering radius is 1.5× dimension of the element.

In the following examples, $p = 3$ *is* used.

5.1 Buckling and eigenvalue analysis

To ensure that the uniform temperature rise does not induce buckling of the initial plate, $T_{cr} = 100.8$ °C is first calculated as the upper limit of ΔT by carrying out an buckling analysis (1). Four thermal cases, i.e. $\Delta T = 0$ °C, 50 °C, 75 °C, 90 °C, are chosen for analysis in this work.

It is shown later that T_{cr} increases as the optimization proceeds, indicating that the plate is always in the pre-buckling state.

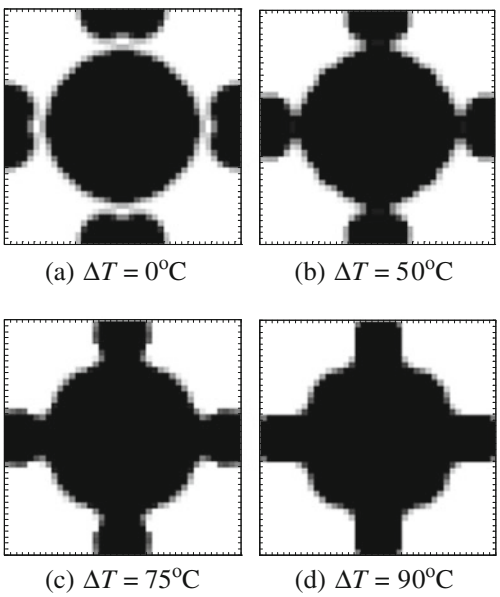

Fig. 6 Topology of the case $f = 250$ Hz (*white*: material 0; *black*: material 1)

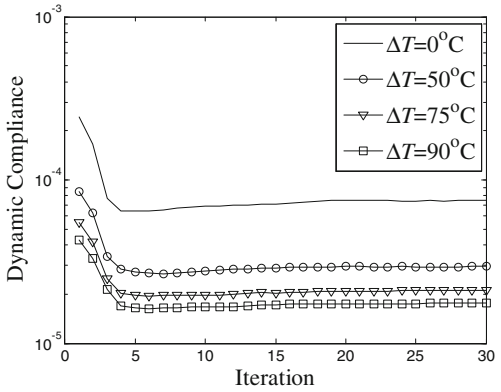

Fig. 7 Iteration history of the dynamic compliance of the case $f = 250$ Hz

The first 15 order frequencies of the initial plate are obtained for the four thermal cases, shown in Fig. 1. It can be found that the natural frequencies decrease as the temperature rises. The fundamental frequencies are 184.2 Hz, 131.8 Hz, 94.4 Hz and 61.3 Hz respectively.

According to the eigenvalue analysis, three excitation frequency cases are selected, that is, $f = 50$ Hz, 250 Hz, 1000 Hz. $f = 50$ Hz is below all the fundamental frequencies of the initial plate in the four thermal environments; $f = 250$ Hz is higher than the fundamental frequencies but lower than the 2nd order frequencies; case $f = 1000$ Hz is a relatively high-frequency case.

5.2 Excitation frequency 50 Hz

First, a case with the excitation frequency $f = 50$ Hz is studied, which is lower than all the four fundamental frequencies. Figure 2 shows the optimal topology of the plate under different thermal conditions. As the temperature rise, some materials (material 1) move from the marginal and central parts to connect the two parts stripily.

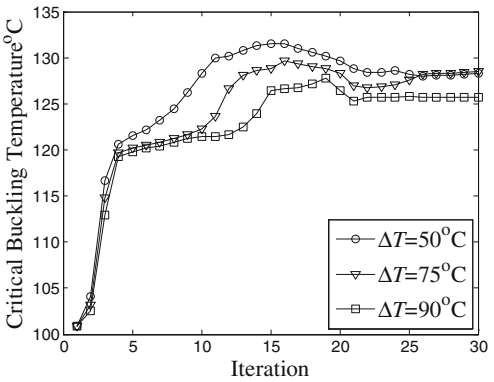

Fig. 8 Iteration history of the critical buckling temperature of the case $f = 250$ Hz

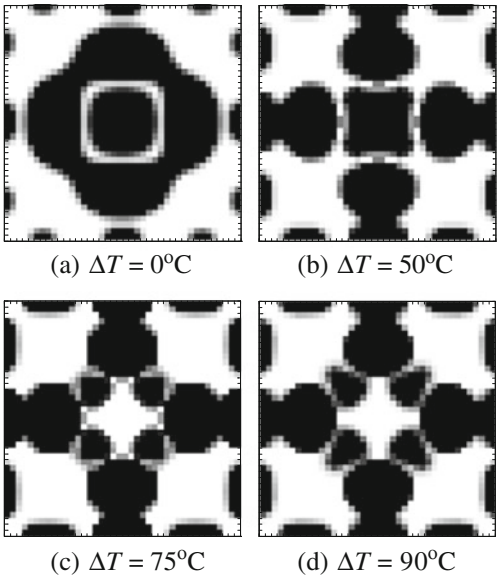

Fig. 9 Topology of the case $f = 1000$ Hz (*white*: material 0; *black*: material 1)

Figure 3 shows that the dynamic compliance of the initial plate is larger for the higher temperature cases, due to that the fundamental frequency is lower and the plate tends to resonance. The dynamic compliance becomes smaller as the iteration grows, since the fundamental frequency increase with respect to the iteration number and the gap between the fundamental frequency and the excitation frequency becomes larger (Fig. 4), which also can be found in Ma et al. (1993), Du and Olhoff (2007a).

Figure 5 shows the iteration history of T_{cr} which increases as the iteration grows, indicating that the plate is always in the pre-buckling state during the optimization process. In some sense, it also means that the optimization yields a "stiffer" thermal structure. T_{cr} is unnecessary to evaluate for the subcase $\Delta T = 0$ °C.

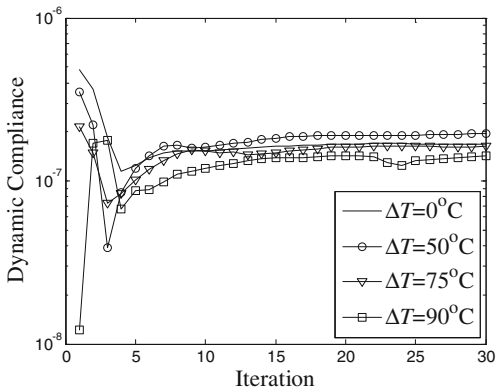

Fig. 10 Iteration history of the dynamic compliance of the case $f = 1000$ Hz

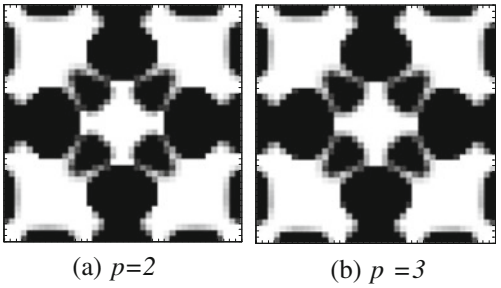

Fig. 11 Topology of the case $f = 1000$ Hz and $\Delta T = 90$ °C (*white*: material 0; *black*: material 1)

5.3 Excitation frequency 250 Hz

Figure 6 shows that the optimal topology of the case $f = 250$ Hz. It can be seen that as the temperature rise, the marginal parts gradually become ribbonlike, which is a bit similar to that of the case $f = 50$ Hz.

Figure 7 shows that the dynamic compliance of the initial plate is larger for the lower temperature cases, which is quite opposite to the case $f = 50$ Hz. This indicates that the fundamental mode may be the main component that affects the dynamic response. If it is not, according to Fig. 1, the 2nd natural mode would be the main one and the dynamic compliance of the subcase $\Delta T = 90$ °C might be greater than that of the other cases.

Figure 8 shows the iteration history of T_{cr}.

5.4 Excitation frequency 1000 Hz

Figures 9 and 10 show that the optimal topology and the dynamic compliance of the case $f = 1000$ Hz in the four thermal conditions. The topology is more complex than that of the two low-frequency cases. The temperature rise

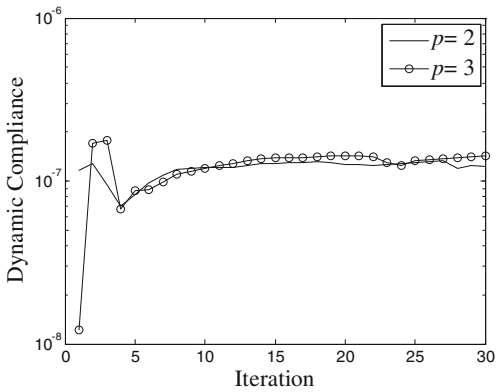

Fig. 12 Iteration history of the dynamic compliance for the case $f = 1000$ Hz and $\Delta T = 90$ °C

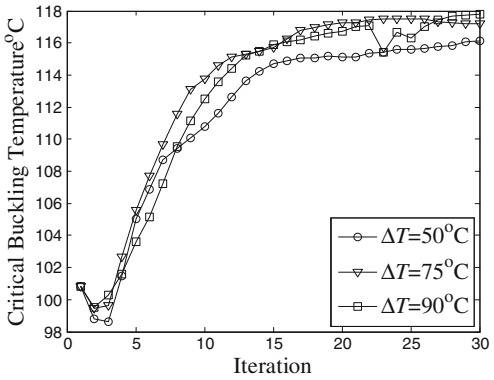

Fig. 13 Iteration history of the critical buckling temperature of the case $f = 1000$ Hz

may significantly change the topology. It is noticed that the final convergent dynamic compliance of the subcase $\Delta T = 90$ °C is larger than the initial value. It is known that the initial compliance is highly related to the factor p, while the optimal structural after optimization is supposed to be independent to the factor (same topology and few gray elements), illustrated in Figs. 11 and 12.

Figure 13 shows the iteration history of T_{cr}.

6 Conclusion

Topology optimization of a thermally stressed bi-material plate in the pre-buckling state is carried out in this paper to minimize the dynamic compliance. The thermal stress induced by the uniform temperature rise changes the dynamic characteristic, thus altering the optimal topology. The thermal dynamic formula is presented in a stress stiffening form. Both direct and adjoint methods are discussed and the latter is employed to keep the computational cost at a relatively low level by avoiding the sensitivity of the thermal displacement (stress). The effect of the thermal environment is investigated though some typical pre-buckling numerical examples.

It is found that when the excitation frequency is below the initial fundamental frequency, i.e. for the case $f = 50$ Hz, the compliance increases as the temperature rises, and some materials moves to connect the marginal and central parts together. For the case $f = 250$ Hz in this research, the effect of the thermal environment on the topology is kind of similar to the $f = 50$ Hz. In both cases, the fundamental mode may be the main component that affects the dynamic response. For the case $f = 1000$ Hz, the topology is more complex than the low-frequency cases, and the temperature rise may significantly change the topology. It is also shown that the plate is always in the pre-buckling state during the optimization.

Acknowledgments The assistance on the GCMMA algorithm from Prof. Svanberg K is gratefully acknowledged. And the constructive comments from the reviewers are also highly appreciated.

References

Bendsøe MP, Kikuchi N (1988) Generating optimal topologies in structural design using a homogenization method. Comput Methods Appl Mech Eng 71(2):197–224. doi:10.1016/0045-7825(88)90086-2

Bendsøe MP, Sigmund O (2003) Topology optimization: theory, methods and applications. Springer, Berlin

Bruyneel M, Duysinx P (2005) Note on topology optimization of continuum structures including self-weight. Struct Multidisc Optim 29(4):245–256. doi:10.1007/s00158-004-0484-y

Cook RD (1994) Finite element modeling for stress analysis. Wiley, New York

Diaz AR, Kikuchi N (1992) Solutions to shape and topology eigenvalue optimization using a homogenization method. Int J Numer Methods Eng 35(7):1487–1502

Du J, Olhoff N (2007a) Minimization of sound radiation from vibrating bi-material structures using topology optimization. Struct Multidisc Optim 33(4–5):305–321. doi:10.1007/s00158-006-0088-9

Du J, Olhoff N (2007b) Topological design of freely vibrating continuum structures for maximum values of simple and multiple eigenfrequencies and frequency gaps. Struct Multidisc Optim 34(2):91–110. doi:10.1007/s00158-007-0101-y

Gao T, Zhang W (2010) Topology optimization involving thermoelastic stress loads. Struct Multidisc Optim 42(5):725–738. doi:10.1007/s00158-010-0527-5

Huang X, Zuo ZH, Xie YM (2010) Evolutionary topological optimization of vibrating continuum structures for natural frequencies. Comput Struct 88(5–6):357–364. doi:10.1016/j.compstruc.2009.11.011

Jog CS (2002) Topology design of structures subjected to periodic loading. J Sound Vib 253(3):687–709. doi:10.1006/jsvi.2001.4075

Kim WY, Grandhi RV, Haney M (2006) Multi objective evolutionary structural optimization using combined static/dynamic control parameters. AIAA J 44(4):794–802. doi:10.2514/1.16971

Li Q, Steven GP, Xie YM (1999) Displacement minimization of thermoelastic structures by evolutionary thickness designs. Comput Methods Appl Mech Eng 179(3–4):361–378. doi:10.1016/S0045-7825(99)00047-X

Ma ZD, Kikuchi N, Hagiwara I (1993) Structural topology and shape optimization for a frequency response problem. Comput Mech 13(3):157–174. doi:10.1007/BF00370133

Ma ZD, Kikuchi N, Cheng HC (1995) Topological design for vibrating structures. Comput Methods Appl Mech Eng 121(1–4):259–280. doi:10.1016/0045-7825(94)00714-X

Min S, Kikuchi N, Park YC, Kim S, Chang S (1999) Optimal topology design of structures under dynamic loads. Struct Optim 17(2–3):208–218. doi:10.1007/BF01195945

Pedersen NL (2000) Maximization of eigenvalues using topology optimization. Struct Multidisc Optim 20(1):2–11, doi:10.1007/s001580050130

Pedersen NL (2001) On topology optimization of plates with prestress. Int J Numer Methods Eng 51:225–239. doi:10.1002/nme.162

Pedersen NL (2002) Topology optimization of laminated plates with prestress. Comput Struct 80:559–570. doi:10.1016/S0045-7949(02)00026-3

Pedersen P, Pedersen NL (2012) Interpolation/penalization applied for strength design of 3D thermoelastic structures. Struct Multidisc Optim 45(6):773–786. doi:10.1007/s00158–011–0755–3

Penmetsa RC, Grandhi RV, Haney M (2006) Topology optimization for an evolutionary design of a thermal protection system. AIAA J 44(11):2664–2671. doi:10.2514/1.15906

Rodrigues H, Fernandes P (1995) A material based model for topology optimization of thermoelastic structures. Int J Numer Methods Eng 38(12):1951–1965. doi:10.1002/nme.1620381202

Rozvany GIN (2001) On design-dependent constraints and singular topologies. Struct Multidisc Optim 21(2):164–172. doi:10.1007/s001580050181

Sigmund O (2001) A 99 line topology optimization code written in matlab. Struct Multidisc Optim 21(2):120–127. doi:10.1007/s001580050176

Stolpe M, Svanberg K (2001) An alternative interpolation scheme for minimum compliance topology optimization. Struct Multidisc Optim 22(2):116–124. doi:10.1007/s001580100129

Svanberg K (1987) The method of moving asymptotes—a new method for structural optimization. Int J Numer Methods Eng 24(2):359–373. doi:10.1016/j.cma.2007.11.013

Svanberg K (1995) A globally convergent version of MMA without linesearch. In: Proc. first world congress of structural and multidisciplinary optimization. Pergamon, Oxford, pp 9–16

Xie YM, Steven GP (1996) Evolutionary structural optimization for dynamic problems. Comput Struct 58(6):1067–1073. doi:10.1016/0045-7949(95)00235-9

Zienkiewicz OC, Taylor RL (2005) The finite element method for solid and structural mechanics, 6th edn. Butterworth–Heinemann, Elsevier, London